A Numerical Prediction of the Hydrodynamic Torque acting on a Safety Butterfly Valve in a Hydro-Electric Power Scheme

A. D. Henderson, J. E. Sargison, G. J. Walker and J. Haynes
School of Engineering
University of Tasmania
Hobart
AUSTRALIA

alan.henderson@utas.edu.au http://www.eng.utas.edu.au

Abstract: - A numerical study of the flow through a safety butterfly valve used in a hydro-electric power scheme to stop water supply to a downstream penstock is reported. Computational fluid dynamics applied in a quasi-steady manner is used to predict the variation in hydrodynamic torque coefficient with opening angle during a constant head test. Factors influencing these results, such as Reynolds number and unsteady flow effects, are found to be significant. The predicted results are compared with field measurements of the full-size valve. Issues associated with applying the numerical results to predict valve characteristics at higher Reynolds numbers are discussed. Further computational and experimental studies are recommended.

Key-Words: - Numerical, Safety, Butterfly valve, Torque, Hydro-electric power

1 Introduction

Hydro-electric power schemes require safety valves to stop water flow from the reservoir to the turbine. Turbines that operate under significant head and have a long penstock usually need a valve near the upstream reservoir to isolate flow to the penstock. Butterfly valves are often chosen for this purpose since they have a simple mechanical construction, fast closing time, and more importantly give a low head loss when fully open (see [1]). The size of these 'hill-top valves' will depend on the size of the penstock section in which they are housed. Larger valves may have diameters up to 5 m.

The valve investigated in this study is installed in a hydro-electric power generating scheme located in central Tasmania, Australia. The valve has a diameter D = 3.048 m and a leaf of convex cross-section. The valve closing mechanism is similar to that described by Ellis and Mualla [2]. The valve is normally in a fully open position. When the valve is triggered by either an abnormally high flow rate, or a remote controlled signal, a locking mechanism disengages. The valve is then subjected to a large out of balance moment imposed by weights that act to close the valve. The closing motion of the valve is regulated using two large oil-filled dashpots. Oil is forced from the dashpot chambers through a small orifice, which gives a smooth and near constant valve closing rate. During a valve closure test, the dashpot pressure, valve position, upstream static head and downstream static head are recorded. The torque acting on the valve is then estimated from the measured dashpot pressure and the mechanical arrangement of the valve.

The torque acting on a closing valve may be resolved into several components (see American Water Works Association (AWWA) [3]): bearing torque (T_b), torque imposed by an offset centre of gravity of the valve (T_{cg}), hydrodynamic torque (T_d), packing torque (T_p), and torque due to hydrostatic pressure (T_h). The sign convention used in this study is for torque to be positive when acting in the closing direction. Components T_b and T_p always act in the opposite direction to the valve closing direction. Components T_d and T_{cg} may act in either direction, depending on geometry [2, 3].

It is common to express the hydrodynamic torque T_d in the form of a dimensionless torque coefficient such as $C_t = T_d / (D^3 \Delta P)$ where ΔP represents the static pressure differential across the valve. AWWA [3] suggests for model testing, that the downstream pressure should be measured at least 10D downstream of the valve to allow for sufficient pressure recovery and the upstream pressure should be measured at least 2D upstream.

A common method of determining the valve torque characteristic of a butterfly valve is by a constant head test as described in AWWA [3]. In

that test, the valve is positioned in a long horizontal section of pipe that is fed by a constant head source. Measurements of torque and head loss are then made at various valve angles.

The actual head-flow characteristic will differ from that in such simple model tests because there will be greater operating head, additional head loss components due to penstock friction, bends and transitions; and also a head drop across the turbine. In an actual test, the turbine head reduces as the valve closes, leading to very low pressure behind the valve. To prevent buckling collapse of the penstock, anti-vacuum valves located a short distance downstream from the valve admit air into the penstock tunnel when the pressure drops below atmospheric. This is also known to reduce the severity of cavitation [3, 4]. Owing to these factors, the maximum hydrodynamic torque will occur at a greater valve angle than predicted in a constant head test. Nonetheless, the dimensionless torque coefficient should only differ due to departure from similarity conditions. Numerous studies involving model testing of butterfly valves [1, 5–7] show that the flow-induced torque coefficient approaches a constant value at high Reynolds number. For this reason, AWWA [3] recommends a minimum Reynolds number $Re_D = \rho\bar{u}D/\mu$ for model testing of 10^5, where $\bar{u}$ is the mean penstock velocity, ρ is density and μ is dynamic viscosity.

3 Scope of Investigation

3.1 Valve Geometry

A schematic diagram of the valve geometry at mid-section is shown in Fig. 1. The valve is symmetrical about the Y′−Z and X′−Z planes and maintains a uniform maximum leaf section thickness t of 510 mm along much of its axis. A small tip gap of 4 mm is sealed by a circular rubber seal. Other details of the valve geometry were provided by Barnbaum [8].

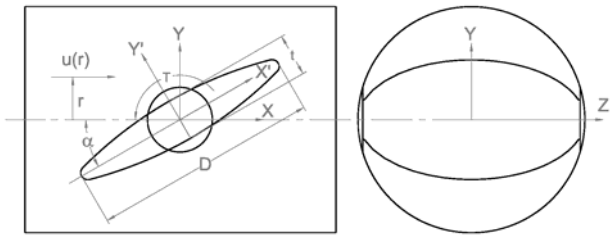

Fig. 1: Butterfly valve arrangement: mid-section view (left) and upstream view (right)

3.2 Flow Conditions

The valve is situated in a long straight circular section of steel pipeline and operates under a static head relative to atmospheric pressure of approximately 65 m. Two flow rate cases were selected to match the field measurements available.

Case	Q (m^3/s)	Re_D (10^6)	$\bar{u}$ (m/s)
A	21.2	8.8	2.91
B	35.3	14.7	4.84

Table 1: Full-scale flow conditions

3.3 Numerical Model

A quasi-steady modelling approach was used in this study, in which steady flow solutions were obtained at various valve angles. This was deemed to be acceptable given the long valve closing time of 6 minutes relative to the flow transit of a few seconds. The valve tip speed at mid-plane was at least 2 orders of magnitude lower than the upstream flow speed u for the higher flow rate in Case B. However, the velocity around the valve tip is considerably faster than in the upstream flow. It was recognised that the system does not respond instantly to a change in flow conditions, as it takes approximately 1.5 s for pressure waves to travel from the valve to the penstock inlet, and approximately 4 s for waves to travel from the valve to the turbines. Dynamic effects would become significant at high valve angles where the rate of reduction in flow area with time becomes large. The experimental results provided by Barnbaum [8] showed evidence of this by a surge in upstream head when the valve angle α had reached about 60°.

The commercial code ANSYS CFX was used for the analysis. The valve geometry was created using SolidEdge software and then imported into ANSYS Design Modeller. The flow was assumed to be symmetrical about the valve X−Y centreplane, and thus only half of the flow field was modelled by applying a symmetry boundary condition. Further details of the geometry creation are given in Henderson et al. [9].

Only the initial flow rate with the valve fully open (α = 0°) was measured in the field testing. As a result, the modelling aimed to simulate a constant head test commonly used to determine valve characteristics [3]. Since defining a velocity profile at the model inlet would set the flow rate and the head loss across the valve, it was decided to instead model a long upstream section of penstock and specify the total pressure at inlet, thereby allowing the velocity profile to develop before

reaching the valve. This distance required for the flow to fully develop may be estimated using an empirical formula for entry L_e length given by Munson [10] as $L_e/D = 4.4(\mathrm{Re}_D)^{1/6}$. This correlation predicts lengths of approximately 56*D* and 60*D* for Cases A and B respectively. Following this it was decided to make the upstream section of penstock 60*D* upstream from the valve axis and the downstream section 15*D* downstream from the valve axis.

The total pressure at inlet was set to give the desired flow rate at fully open condition (α = 0°) and this was then maintained for solutions at other valve angles, allowing the flow rate to decrease accordingly with head loss imposed by the valve.

The computational domain was divided into three main sections: upstream penstock, near valve section, and the downstream penstock. Upstream and downstream penstock sections were meshed using an inflated layer of hexahedral elements on the walls, with triangular-based prism elements in the centre. A layer of inflated elements was used on the valve face to improve modelling of the boundary layer. The surrounding mesh consisted of tetrahedral elements. Meshes were generated for valve angles between 0° and 80° in steps of 10°. The total number of elements contained in each mesh varied between 2.2×10^6 and 2.8×10^6.

The Shear Stress Transport (SST) turbulence model was used for turbulent closure as it is well regarded in prediction of flow separation in an adverse pressure gradient [11]. Studies of Lin and Schohl [12] and Leutwyler and Dalton [13] found that the SST model produced best agreement with experimental measurements of flow-induced loading and torques acting on butterfly valves.

The near wall flow was modelled using 'automatic' wall functions, which automatically switch between a low Reynolds number approach to scalable wall functions depending on local conditions and the wall normal element spacing [11]. The y^+ values of the mesh varied with both inlet Reynolds number and valve angle, but were around 20 on the valve surface and within the specifications given in the software documentation [11]. A high resolution advection scheme was used (see [11]). The six equations solved were *u*, *v* and *w*-momentum equations, conservation of mass, and turbulent kinetic energy (*k*) and frequency (ω).

A convergence criterion for maximum RMS residual of 10^{-6} was set, which is two orders of magnitude below the default convergence level of the solver [11]. Solution times were generally around 15−20 hours using 4 processors of a SGI ALTIX 4700 system (Itanium 2, 1.6 GHz).

4 Results

4.0 Convergence

The target convergence level was not achieved in all cases. An acceptable convergence level was achieved in all cases except for α = 20° and α = 30°. Oscillations were observed in the residuals for those cases, which can be indicative of unsteady flow behaviour. Those cases were restarted as transient simulations and the residuals then reduced to the target convergence criterion. Further details of that study are given in Henderson et al. [9].

4.1 Inlet Velocity Profile

The upstream velocity profile was compared against the widely used power law to verify that the flow had developed by the time it reached the valve. The power law may be expressed as

$$u / u_{\max} = \left(1 - r / R\right)^{1/n} \qquad (1)$$

where the index *n* was determined by applying a curve fit to the predicted velocity profile. These were determined as 10.5 and 11.4 for Cases A and B respectively. Schlichting [14] used this approach to determine indices for smooth pipe flow data at lower Reynolds numbers than those considered in this study. Predicting the index *n* by extrapolating Schlichting's results to the higher Reynolds numbers given in Table 1 yields similar results of 10.8 and 11.2 for Cases A and B respectively.

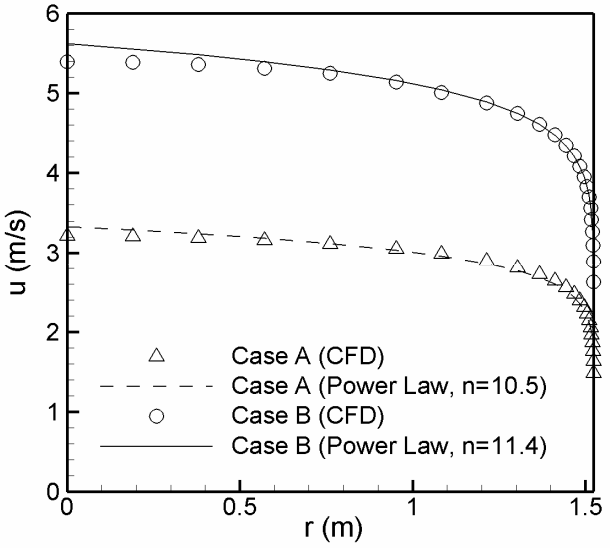

Fig. 2: Velocity distribution 2.1D upstream from the valve axis (α = 0°).

Fig. 2 compares the predicted velocity profile from the CFD and power law at a location 2.1*D* axially upstream from the valve shaft axis for α = 0°. Reasonable agreement is observed in the near-wall region, but this deteriorates slightly toward the centre as expected. It is possible that the flow has not fully developed, although Schlichting [14] shows that the power law becomes increasingly inaccurate towards the centre of the flow ($r/R < 0.2$) and produces an unrealistic velocity gradient at the centre. Further increasing the length of upstream penstock was deemed unnecessary for this study. The profile was also checked at a distance of 4.2*D* upstream from the valve axis. The maximum difference between profiles was less than $0.02\bar{u}$ which confirms that there was no significant upstream influence of the valve at these positions.

4.2 Mesh Resolution

A mesh refinement study for Case B is described in Henderson et al. [9]. The mesh was coarsened equally in all directions for each subsequent trial. The number of elements in the inflated wall layer was changed to maintain an acceptable aspect ratio. However, the first element height and expansion ratio of the inflated wall layers were not changed as the resolution was already adequate to model the boundary layer. The results suggest that sufficient resolution was provided by the mesh of around 2×10^6 elements used for the purposes of this study.

4.3 Description of Flow Field

A sequence of plots showing the mid-valve flow field on the X-Y symmetry plane for Case B is shown in Fig. 3. The velocity magnitude shown in each plot has been normalised by the local maximum velocity u_{max}. At α = 10°, there is no separation observed at mid-plane. Although not shown, a small region of separated flow forms behind the valve close to the wall. For α = 20° a small separation forms at mid-plane but the flow appears to reattach. The extent of this separation increases with valve angle, so that most of the downstream valve surface is separated at α = 40°. Further increasing the valve angle increases the extent of the downstream flow separation. Despite this, the downstream length of flow domain was sufficiently long to prevent reverse flow at the outlet.

A dominant feature of the downstream flow is a counter-rotating streamwise vortex pair that develops at all non-zero valve angles. Since the valve is at an angle to the upstream flow, the pressure differential across the valve directs fluid downward near the sides, creating a swirling flow.

The strong vortical flows persists throughout the whole downstream flow domain. They represent tip vortices associated with the lift force perpendicular to the pipe axis acting on the valve leaf. A visualisation of this flow is shown in Fig. 4.

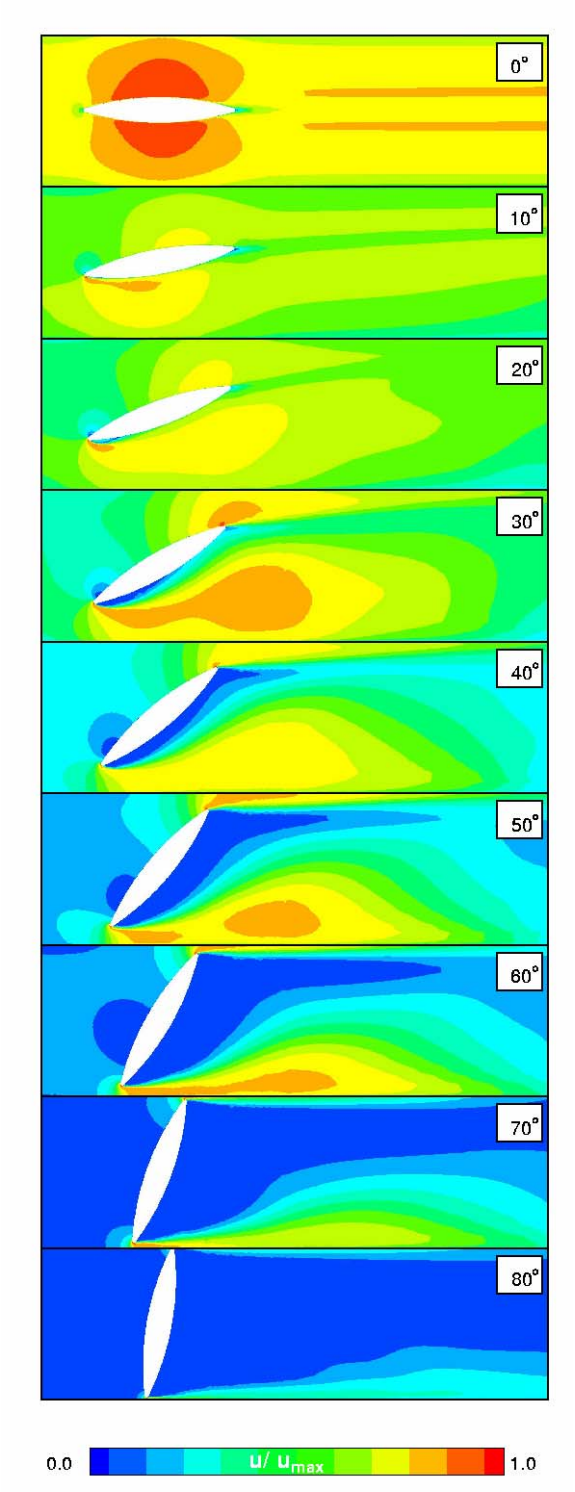

Fig. 3: Contours of u/u_{max} for various valve angles (α) shown on the X-Y symmetry plane for Case B.

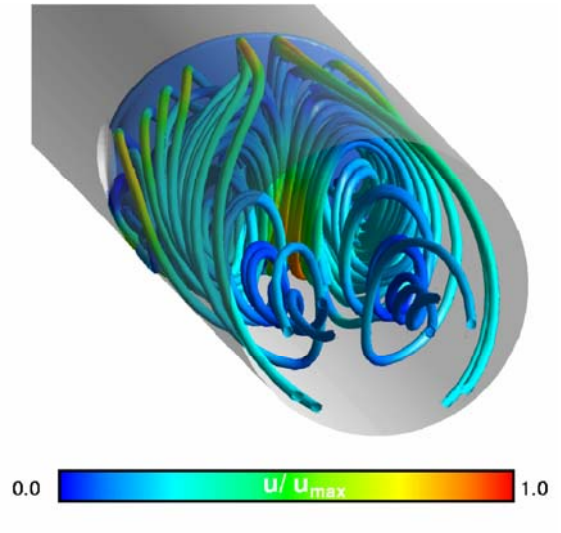

Fig. 4: Pathlines downstream for Case B at α = 60°

4.4 Unsteady Flow Effects

The flow behind the valve is known to be unsteady. Leutwyler and Dalton [13] note that for valve angles less than about 70° the flow downstream from the valve is dominated by strong unsteady vortical disturbances. This is caused by flow separation at the leading edge of the downstream face of the disk and the large diffusion of the flow around the downstream side of the valve. The vortical disturbances were reported to cause fluctuations in pressure, force and torque acting on the valve.

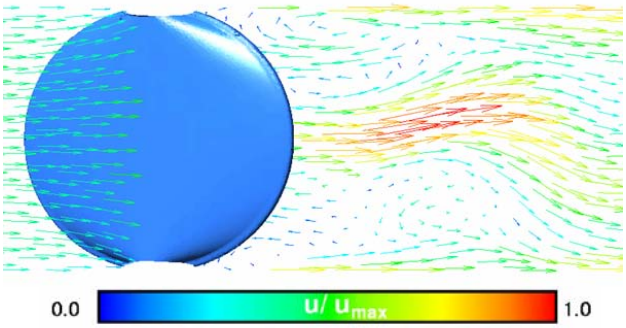

Fig. 5: Instantaneous velocity vectors on a X-Z plane for Case B at α = 30°.

The transient calculations showed oscillations in torque coefficient with a frequency of around 1 Hz. For regular vortex shedding behind a bluff body with a Strouhal number of St = 0.2, we would expect an eddy shedding frequency of about 1.3 Hz. The convergence of the steady solution was clearly hampered by unsteady flow, but it nonetheless reached a value close to the average in the unsteady flow solution (see [9]). A transient solution using the whole model (no symmetry) showed that the eddy shedding alternates between sides. Despite this modified flow pattern, C_t did not significantly change from symmetrical case. Fig. 5 shows an instantaneous view of the flow pattern.

4.5 Reynolds Number Dependence

Solutions over a range of Reynolds numbers were obtained at two valve positions to investigate Reynolds number effects. The torque coefficient was found to increase at high Reynolds numbers. At a valve angle of α = 10°, C_f increased by 14% between $Re_D = 6\times10^6$ and $Re_D = 15\times10^6$. A similar finding was made by Solliec and Danbon [7] in model valve tests at $Re_D = 7\times10^5$. It is likely that changes in upstream velocity profile with Reynolds number are a contributing factor.

4.6 Comparison with Field Measurements

Data from valve closure tests were provided by Hydro Tasmania (Barnbaum [8]). In order to determine the hydrodynamic torque component from the total torque estimate, the total torque was corrected using data from a still water test. This approach aimed to remove many torque components common to both the still water and flow closure tests. Common components include T_{cg}, T_h, and to some extent T_b and T_p, but additional bearing friction induced by hydrodynamic loading would not be accounted for. The correction was applied using $T_d \approx T(1\text{-}P^*/P)$, where T is the torque estimated from the pressure measured in the dashpots, P is the dashpots pressure, and P^* is the dashpots pressure during a still-water test.

Fig. 6 compares predicted and measured valve torque characteristics. The curves qualitatively agree in terms of shape and sign, with maximum torque coefficient occurring near α = 20°. However the maximum torque values from the experimental results are approximately 25% less than predicted at α = 20°. This difference may partially be explained by two main factors. First, there will be friction in mechanical connections and viscous losses in the oil filled dashpots that are not accounted for in the torque estimation. Second, the bearing friction would be expected to increase as hydrodynamic loading is increased. Both factors would contribute to reduce the indicated experimental torque below the actual experimental torque. Other contributing factors such as cavitation and air admission will alter the flow pattern around the valve and consequently the torque acting on the valve,

although these effects are largely suppressed by the large upstream head and would only occur for $\alpha >$ 55°.

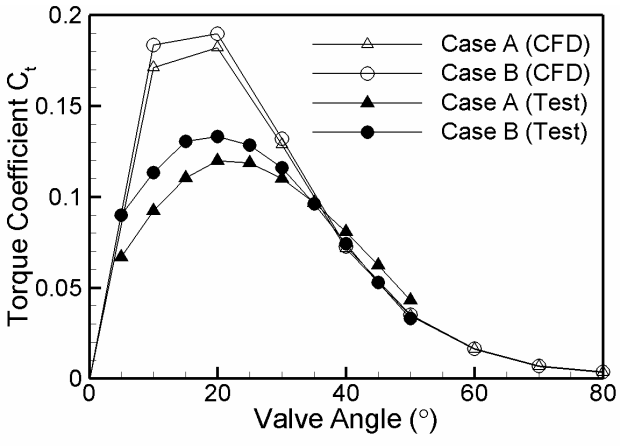

Fig. 6: Measured and predicted torque coefficient

Differences due to Reynolds number effects will arise from differences between the actual head flow characteristic and constant head approximation used in the CFD model.

5 Conclusion

This study has described a numerical study of the flow though a safety butterfly valve. The results showed that a strong vortical flow pattern develops downstream from the valve, and that the flow is highly unsteady over an intermediate range of valve angles. The shape and sign of the predicted torque characteristic agreed with experimental field measurements, although the maximum values are greater. The study highlights the need for improved field measurements that include measurement of flow rate. This would enable CFD simulations to be performed at more representative conditions. Unsteady data from a scale model of the valve would also assist in validating the CFD model and also provide accurate data of cavitation onset.

6 Acknowledgements

The Authors would like to thank Garth Barnbaum at Hydro Tasmania for helpful comments and suggestions and for provision of the field test data. The Authors are also grateful to the Tasmanian Partnership for Advanced Computing (TPAC) for providing the computer resources necessary for this study.

References

[1] Gaden, D., A contribution to the study of butterfly valves. part 1, *Water Power*, 55, 1951, 456–474.

[2] Ellis, J. and Mualla,W., Dynamic behaviour of safety butterfly valves, *Water Power and Dam Construction*, 121, 1984, 26–31.

[3] American Water Works Association (AWWA), Butterfly valves: Torque, head loss and cavitation analysis, Technical Report M49, American Water Works Association, 2001.

[4] Tullis, J. P., Hydraulics of Pipelines. Pumps, Valves, Cavitation, Transients, John Wiley and Sons Inc, New York , 1989.

[5] Danbon, F. and Solliec, C., Aerodynamic torque of a butterfly valve—influence of an elbow on time-mean and instantaneous aerodynamic torque, *ASME Journal of Fluids Engineering*, 122, 2000, 337–344.

[6] MacLellan, D. A. and Caruthers, J. H., Hydraulic characteristics and limitations of butterfly valves for flow control, in Glenfield Gazette. Valve Symposium— 'Fluid Control in Industry', London, May 1–3, 2001, 9pp.

[7] Solliec, C. and Danbon, F., Aerodynamic torque acting on a butterfly valve. Comparison and choice of a torque coefficient, *Journal of Fluids Engineering*, 121, 1999, 914–917.

[8] Barnbaum, G., Valve drawings and closure test report, Private comm. to J. Haynes, 2006.

[9] Henderson A. D., Sargison, J. E., and Walker, G. J., A Numerical Study of the Flow through a Safety Butterfly Valve in a Hydro-Electric Power Scheme, In Proceedings of 16th Australasian Fluid Mechanics Conference, December 2 -7, Gold Cost, Australia, 2007.

[10] Munson, B. R., Young, D. F. and Okiishi, T. H., Fundamentals of Fluid Mechanics, John Wiley Inc, 2002, fourth edition.

[11] ANSYS Europe Ltd, ANSYS CFX V11 solver modeling guide, 2007.

[12] Lin, F. and Schohl, G. A., CFD prediction and validation of butterfly valve hydrodynamic forces, In Conference Proceedings of World Water and Environmental Resources Congress, Editors G. Sehlke, D. Hayes and D. Stevens, 27 June – 1 July, Salt Lake City, USA, 2004.

[13] Leutwyler, Z. and Dalton, C., A computational study of torque and forces due to compressible flow on a butterfly valve disk in mid-stroke position, *ASME Journal of Fluids Engineering*, 128, 2006, 1074–1088.

[14] Schlichting, H., Boundary-Layer Theory, McGraw–Hill, 1968, 6th edition.